HardwareX 20 (2024) e00596

Contents lists available at ScienceDirect

HardwareX

journal homepage: www.elsevier.com/locate/ohx

A multispectral camera in the VIS–NIR equipped with thermal imaging and environmental sensors for non invasive analysis in precision agriculture

Dumitru Scutelnic [a,*], Riccardo Muradore [b], Claudia Daffara [a]

[a] Department of Computer Science, University of Verona, Italy
[b] Department of Engineering for Innovation Medicine, University of Verona, Italy

A R T I C L E I N F O

Keywords:
Multispectral camera
Thermography
Non-destructive technique
Smart farming
Precision agriculture
Plant disease detection
Agritech

A B S T R A C T

Multispectral imaging (MSI) is a technique used to inspect materials properties in different domains, ranging from industrial to medical and cultural heritage and, recently, precision agriculture. Even though several MSI solutions are already commercially available, the research community is working to optimize multispectral cameras in terms of performance and cost. Systems for the agricultural field are usually very compact, combined with drones for large areas acquisition. In this work, we detail the implementation of an innovative, modular and low-cost solution of a multispectral camera based on three core camera systems in the optical (VIS–NIR) and thermal (LWIR) range. Multispectral imaging is performed with a rotating wheel of interchangeable band-pass filters. The system is also equipped with a set of environmental sensors to acquire CO_2 concentration values, light intensity, temperature, and relative humidity of the surrounding environment. The technology and the measurement protocol were experimentally validated in laboratory and in open field. Advantages with respect to the available MSI cameras mounted on UAV is the integrated imaging in both the reflectance and the thermal emissive band in a close-up imaging setup and the use of environmental sensors. From the multispectral stack the spectral signature of the plants can be obtained and various vegetation indices (e.g., NDVI, NDRE) can be calculated for investigating the health status of the plant, while thermography provide additional monitoring. Close-up multispectral imaging is expected to tackle the new challenges of precision agriculture by enabling the acquisition of high-quality dataset on single plants.

Specifications table

Hardware name	Multispectral camera (MSX)
Subject area	• Non Destructive Testing (NDT) • Engineering and Material Science • Environmental, planetary and agricultural sciences

* Corresponding author.
E-mail address: dumitru.scutelnic@univr.it (D. Scutelnic).

https://doi.org/10.1016/j.ohx.2024.e00596
Received 22 May 2024; Received in revised form 30 September 2024; Accepted 9 October 2024

Available online 21 October 2024

Hardware type	• Imaging tools • Measuring physical properties and in-lab sensors • Field measurements and sensors • Electrical engineering and computer science
Closest commercial analog	Phase One Rainbow Multispectral Imaging Solution, Muses9 multispectral-cameras and SpectroCam™ Multispectral Wheel Camera
Open source license	CERN-OHL-S
Cost of hardware	Approx. 3000 €
Source file repository	https://zenodo.org/doi/10.5281/zenodo.10052826

1. Hardware in context

Climate change strongly affects traditional agriculture due to extreme events and to the spreading of diseases related to the increasing temperature. The combination of these factors leads to a reduction in the volume and quality of harvests. For these reasons, the adoption and development of new technologies in agriculture has become increasingly essential to maintain or improve food volume and quality, as the world population is expected to grow to 10 billion by 2050 [1].

Today, more efficient farming methods exist, such as vertical farming, hydroponics, agrovoltaic, and precision farming. With the advent of smart farming, there is a need to collect as much valuable data as possible through various technologies and sensors for remote and field monitoring of the multiple parameters crucial to plant growth and harvest prediction. Robotic vehicles, such as unmanned aerial vehicles (UAVs) endowed with sensors/actuators, capable of assessing plant indices or optimally distributing products over entire fields in a short time, are increasingly adopted. In addition, unmanned ground vehicles (UGVs) are being developed to identify and remove weeds, harvest ripe crops autonomously, and monitor the cultures locally. The ultimate goals are to increase production, optimize the use of valuable resources such as water, soil, fertilizers, and reduce the use of chemical fertilizers and pesticides as much as possible [2].

Multispectral and thermographic technologies have long been known in various fields of application: industrial [3], medical, and cultural heritage [4–7], and only recently in the agri-food sector [8]. These imaging technologies estimate various vegetation indices such as NDVI, NDRE, CWSI, etc, [9–12]. through which it is possible to assess the health status of plants, the lack of nutrients or water, and the optimal sunlight [13]. However, to date, well-established methods and technologies still need to be available to the farmer to estimate the presence of pests and diseases on plants. One of the key factors for preventing yield and quantity losses in agricultural products is the early identification of such diseases. It is difficult to do manually and would require much time and an expert eye to identify and classify plant diseases. For this reason, a multispectral imaging system able to automate the acquisition, image processing, and classification using artificial intelligence (AI) would greatly help speed up the time for analysis. AI algorithms trained on a large amount of data are expected to have a better analytical sensitivity than experts. Symptoms of the disease are observed on the stem and on the fruits, but in most cases, they are on the leaves, showing as colored spots or streaks. They are the main visible symptoms when the plant becomes diseased. Some research has been done to isolate sensitive wavelengths useful for estimating plant diseases, but unfortunately, the studies are still very preliminary [14].

To date, we find several manufacturers of multispectral cameras for agricultural applications, using multiple imaging sensors and optics, each dedicated to a specific spectral band. Table 1 reports a comparison of the available systems; the prototype presented in this work is also reported. Most of these multispectral cameras are very compact and lightweight, with a fixed and small number of spectral bands acquired by different sensors at the same time, as they are designed to be used on UAVs and survey large areas [15]. The main disadvantages of this approach are the use of small imaging sensors, consequently with lower material quality, lower sensitivity and lower spatial resolution, and a fixed focal length set at infinity. Morales et al. [16] have implemented a compact and low-cost systems based on a single-sensor coupled to a filter wheel. Drones have long been on the market compared to rovers and, consequently, are the most popular and marketed means of doing multispectral imaging for agriculture applications. However, aerial imaging can only provide the global evolution of the mean status of a field; in order to acquire more detailed data on the status of single plants close imaging mounted on rovers is necessary.

Multispectral imaging by filter wheel has been used in different fields, e.g., medical [5], industrial [17,18], cultural heritage [19], agriculture [16]. Alternative methods in agriculture involve patterned filters aligned with the sensor to acquire VIS and NIR in-band images [20]. A specific approach, recently demonstrated, couples multiband filtering and color camera to concurrently acquire multiple spectral images [21,22]. The mentioned approaches are fascinating and based on valuable ideas, but to date, there is a lack of multispectral imaging systems optimized for close imaging of plants and able to acquire datasets at high spatial resolution suitable for precision agriculture.

In this work, we aimed to design and build an innovative multispectral camera, which incorporates imaging and environmental sensors in a single system. Specifically, our triple-camera system consist of on three imaging sensors, i.e., an RGB array in the visible (VIS) range, a monochrome sensor with high sensitivity in the near infrared (NIR), a thermal sensor based on microbolometer array sensible in the long-wave infrared (LWIR). This system is also equipped with four sensors for detecting essential environmental conditions, as temperature T(°C), relative humidity RH(%), light intensity (lux) and CO_2(ppm). The implemented multispectral

Table 1
Summary of multispectral camera for agriculture applications.

Company	Model	Nr. of bands	Thermal sensor	Cost (EUR)
Parrot	SEQUOIA+	2 VIS, 2 NIR + RGB	No	4500
Sentera	Quad	1 VIS, 2 NIR + RGB	No	5000
Sentera	6X Sensor	2 VIS, 2 NIR + RGB	Yes	10 000
MicaSens	REDEDGE-MX	3 VIS, 2 NIR	No	5000
MicaSens	REDEDGE-P	3 VIS, 2 NIR + RGB	No	8000
MicaSens	ALTUM-PT	3 VIS, 2 NIR + RGB	Yes	16 000
SlantRange	4P+	1 VIS, 2 NIR + RGB	No	4000
DJI	P4	3 VIS, 2 NIR + RGB	No	6000
Morales [16]	Filter wheel	3 VIS, 2 NIR	No	2000
MSX (this work)	Filter wheel	6 VIS, 5 NIR	Yes	3000

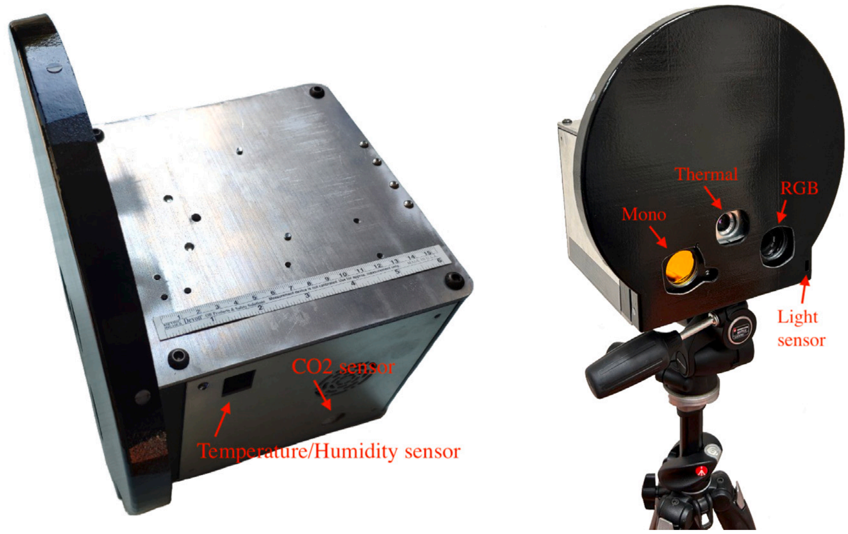

Fig. 1. The multispectral camera with a filter wheel and environmental sensors for measuring temperature (°C), relative humidity (%), dioxide of carbon (ppm) and light intensity (lux).

camera, named MSX, is shown in Fig. 1. It can be used in different environments: indoors (laboratory, greenhouse) and outdoors (open field), with the possibility of being mounted on a tripod, agricultural vehicle, UGV or UAV. The main application of this camera is in the agriculture field, to detect plant stress from nutrition, maturity status of crop, or early detection of plant diseases. The underpinning idea is that plants are dynamic systems that respond to the environment, and our camera provides a more comprehensive monitoring.

The advantages of the system are the use of high-performance sensors, lenses, and images acquired over the same field of view with high spatial resolution and spectral sensitivity. This flexible system allows to use the combination of filters which is the most effective for a specific application. The main disadvantages of a filter wheel-based system lies in the time it takes to acquire all the images, and in its higher dimensions and weight. Table 1 reports also the cost/performance comparison with the available systems for agriculture application, showing that the proposed camera is competitive. It is worth mentioning that our camera can be a low-cost alternative system for nondestructive testing applications in the industrial and cultural heritage fields, where multispectral systems based on single CMOS sensor and filter wheels are typically used, with costs ranging from 10k to 100k euros.

It is worth maintaining that this new type of multispectral camera can also be used in other fields of application, from industry to the heritage sector.

2. Hardware description

The approach to designing the multispectral camera prototype MSX is mainly based on the following key aspects: performance, modularity, and low-cost. Performance refers to the combination of VIS–NIR and thermal imaging sensors, and sensors for environmental measurements, all integrated into a conceptually innovative triple-camera system. Modularity refers to the fact that each component can be easily replaced. The trade off between of cost and spatial resolution and spectral sensitivity is the optimal compromise that makes it attractive for users who could benefit of this device.

The multispectral camera is composed by a rotating filter wheel, and sensors for multispectral imaging. A single image sensor is used to collect images on different wavelengths instead of having one sensor for each filter. Furthermore, the wheel solution allows

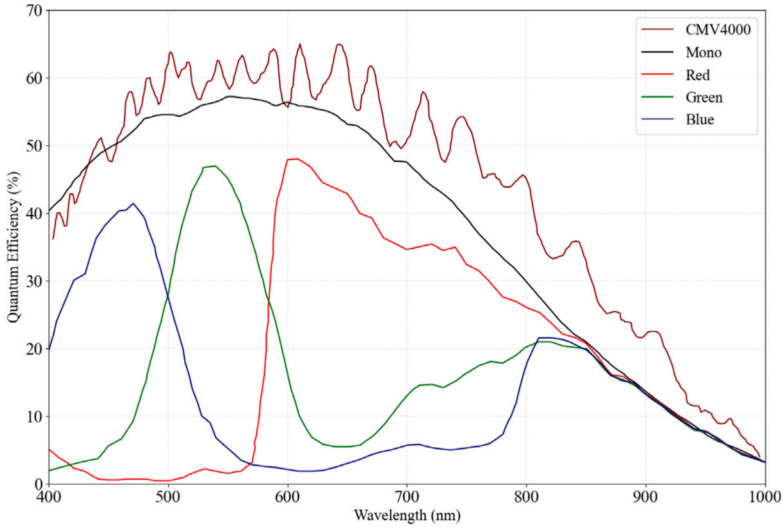

Fig. 2. Quantum efficiency of different types of CMOS sensors, where Basler CMV4000 is a monochromatic sensor with NIR enhancing, Mono is a monochromatic sensor, while Red, Green, and Blue are RGB sensor components, respectively. (For interpretation of the references to color in this figure legend, the reader is referred to the web version of this article.)

us to replace the optical filters installed in the wheel easily or to change the wheel to another one with a different number of filters. The side effect is that acquiring all the images at the available 11 wavelengths takes about 60 s.

2.1. Multispectral camera development: sensors and components description

The multispectral camera consists of two main parts: a circular-shaped front part, where the wheel with the filters is located, and a cubic-shaped rear part housing all the imaging and environmental sensors T, RH, lux and CO_2.

The monochrome camera Basler model aca2040-90umNIR was chosen as the primary sensor for multispectral imaging acquisition. This camera has an array resolution of 4.4 MegaPixels. It is equipped with a CMOS CMV4000 NIR-enhanced monochrome sensor with high quantum sensitivity compared to other CMOS sensors, as shown in Fig. 2. The sensor size is 11.26 mm × 11.26 mm, the pixel size is 5.5 μm × 5.5 μm, the sensor format is 1", the lens mount is C-mount, and the pixel bit depth is RAW12/10/8-bits. The wavelengths to which CMOS sensors are typically sensitive are in the range 400 nm to 1000 nm.

To date, CMOS sensors approach the high performance of CCDs but with a lower cost due in large part to a lower complexity in their production. For this reason, we mostly find CMOS with different characteristics on the market. Sensors with higher resolution or better quality and quantum sensitivity, together with the possibility to control the sensor, drive up the price. Some manufacturers provide an application programming interface (API) for easy integration and programming, which offers full accessibility to all sensor control parameters and access to the raw data. As we have chosen one of the best CMOS sensors in terms of performance, it consequently represents the highest contribution to the cost of the multispectral camera.

Since it is helpful to have also a color image for easing data interpretation, we integrate a second RGB format sensor, Raspberry Pi High-Quality Camera, equipped with Sony's CMOS sensor model IMX477 with Bayer matrix, which has a good price/quality ratio. This camera module has 12.3 megapixels, a lens sensor format of 1/2.3", a diagonal image size of 7.9 mm, and a pixel size of 1.55 μm × 1.55 μm. It has back-illuminated sensor architecture with adjustable back focus and is available with C/CS mount or M12 mount; moreover, an IR cut filter is integrated, and the images available formats are RAW12/10/8-bits.

A thermal sensor was also integrated into the MSX camera, namely a Microbolometer LWIR Mosaic Core manufactured by Seek Thermal. It has an array resolution of 320 × 240 pixels, with a sensitivity between 7.8 μm to 14 μm, a temperature measurement range between −40 °C and 330 °C, and a thermal sensitivity of less than 100 mK.

Several environmental sensors are installed in the MSX camera. To measure the air temperature and humidity, we choose the DHT22 AM2302 sensor. This sensor can measure temperature in the range −40 °C to 80 °C and relative humidity from 0% to 100%; it is recommended to be placed in a shady place with good air circulation. For what concern the measure of light intensity and CO_2, we integrate the BH1750 light sensor that can measure in the range 1 lux to 65 535 lux and the SEN0159 sensor (0 ppm to 10 000 ppm), respectively.

The light sensor in the greenhouse can help farmers to measure the light saturation point and light compensation point of plant growth, and so then adjusting the light intensity when needed in order to enhance crop growth and quality.

Higher CO_2 concentration in the environment increases the photosynthesis process in plants (e.g., wheat, rice, potatoes, barley), leading to greater carbohydrates and biomass production. On the one hand, this process leads to higher crop yields, but on the other hand, to lower nutritional quality, as the plants accumulate more carbohydrates and fewer minerals (e.g., iron and zinc) [23,24].

Table 2
Comparison between main features of commercial single board computer.

Features	Jetson Nano	Raspberry Pi 4	Odroid XU4
Processor	128-core Maxwell GPU, NVIDIA Quad-Core ARM Cortex-A57 @1.43 GHz	Broadcom BCM2711 Quad-Core Cortex-A72 (ARM v8) 64-bit @1.5 GHz	Samsung Exynos5422 8-Core Cortex A15 Quad @2 GHz
RAM	4GB (LPDDR4)	2GB, 4GB or 8GB (LPDDR4)	2GB (LPDDR3)
Gflops	472	24	102.4
Ethernet	Gigabit	Gigabit	Gigabit
Connectivity	Bluetooth/Wifi	Bluetooth/Wifi	Bluetooth/Wifi
Power	5 V/4 A	5 V/3 A	5 V/4 A
Price	≥ 100 €	≥ 35 €	≥ 50 €

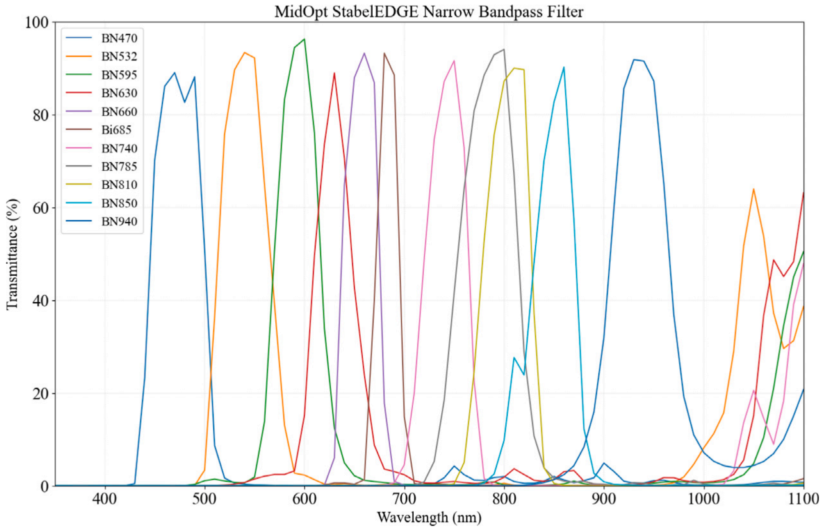

Fig. 3. Filter transmittance curves in the UV–VIS–NIR range measured with the optical spectrometer. (For interpretation of the references to color in this figure legend, the reader is referred to the web version of this article.)

The advantage of multiple sensors in a single system is that when it is mounted on a vehicle moving within the field, it allows the environmental sensors to acquire data at various points of the interest. Therefore, it is as if we have a network of virtual sensors distributed throughout the field, without the need to install a fixed set of sensors.

2.1.1. Single board computer

The Jetson Nano was chosen as the computation unit to control the sensors and to acquire the images at different spectral bands and the environmental measurements. The Jetson Nano is a single-board computer with a 128-core Maxwell GPU, NVIDIA Quad-Core ARM Cortex-A57 @1.43 GHz processor, and 4 GB of RAM. The board is equipped with wifi, bluetooth, several peripheral ports, like USB, HDMI, and a 40-pin GPIO that allow the exchange of data and control of other devices/sensors via protocols like SPI and I2C.

Table 2 compares the main features of commercial single-board computers, like Jetson Nano, Raspberry Pi, and Odroid XU4.

The Jetson Nano is powered by a converter that outputs a voltage of about 5 V and a maximum current of 4 A from 220 V. The Jetson supplies power to all sensors connected to it. The MSX multispectral camera can be powered by a standard 220 V mains socket or a power station (e.g. Bluetti or Ecoflow). In the greenhouse or open field, we use the Bluetti EB55 Power Station with 700 W and 537 Wh, which has about 8 h of working measurements.

2.1.2. Narrow band pass filters

Band-pass filters are optical windows that can be placed in front of or behind the optics; their function is selecting radiation wavelengths in a specific range depending on the properties of the filter. They can be grouped into two categories: broadband filters and narrow-band filters, depending on the size of the spectral region in which the percentage of photons the filters let through, known as filter transmittance.

Table 3
MidOptics bandpass filters used in the multispectral camera.
Source: https://midopt.com/filters/.

Filter name	Useful range (nm)	Bandwidth (nm)	Transmittance (%)
BN470	460–490	45	$\geq$ 85%
BN532	525–550	55	$\geq$ 85%
BN595	580–610	45	$\geq$ 85%
BN630	625–645	45	$\geq$ 85%
BN660	645–675	40	$\geq$ 85%
Bi685	675–692	25	$\geq$ 90%
BN740	730–755	50	$\geq$ 85%
BN785	770–790	55	$\geq$ 85%
BN810	798–820	50	$\geq$ 85%
BN850	840–865	52	$\geq$ 85%
BN940	928–955	55	$\geq$ 90%

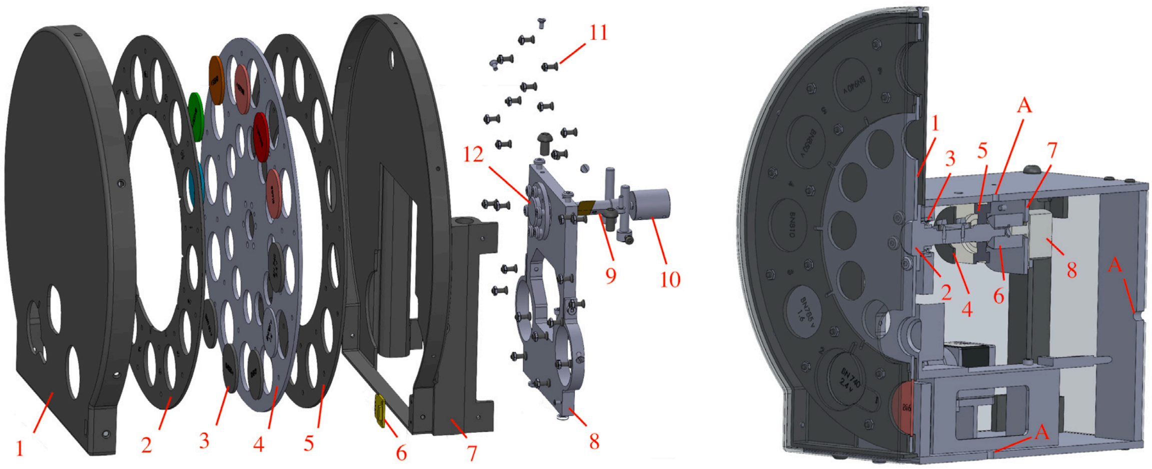

(a) CAD Filter Wheel (b) Motorized System Components

Fig. 4. (a) CAD explosion view of filter wheel components. (1) Front protective cover, (2) Front support structure to hold filters in place, (3) Filters, (4) Aluminum filter wheel structure, (5) Rear support structure to hold filters in place, (6) Light sensor, (7) Back protective cover, (8) Structural support for cameras, cardan and bearing, (9) Cardan, (10) Connector between motor and cardan, (11) Screw to hold the three parts of the filter wheel together, (12) Final cardan structure to attach the wheel. (b) CAD of the filter wheel and motorized system components. (1) Filter wheel, (2) Cardan (3) Support with bearing, (4) Disk with notches for synchronization, (5) Support with bearing, (6) Connector, (7) Motor support for fixing, (8) Stepper Motor (28BYJ-48), (A) 3 out threaded for standard tripod screw.

The spectral transmittance of the MidOptics StablEDGE filters we used for this project was characterized with the OceanOptics HR2000 spectrometer and is shown in Fig. 3. Nominal filter characteristics are listed in Table 3.

Our multispectral system mounts the filters on a wheel in front of the optics; the filters can be easily changed and adapted to the needs of the application, from vegetation and disease indices to pests.

2.1.3. Mechanical structure: filter wheel and motion system

The mechanical structure of the camera that holds all components together was designed with computer-aided design (CAD) software and prototyped with a 3D printer for some elements (in black) and metalwork (in gray).

A rotating filter wheel was designed to hold the filters and position them in front of the camera optics (Mono and RGB). It has a diameter of 240 mm and is equipped with two sets of holes with two different diameters: the first set with 12 holes of 28 mm diameter for the filters and the second set with 12 holes of 22 mm diameter for thermal sensor, located in the central area of the wheel, see Fig. 4(a).

The wheel can hold up to two dozen filters, which are coupled to the monochrome camera. Another position without filter is dedicated to the RGB acquisition (see Fig. 1). Each hole is marked with a number from 1 to 12; by convention, we have placed in the first (1) the BN470 filter and then the filters with increasing bandwidth, up to position 11, which houses the BN980 filter, while position 12 has no filter.

The filter wheel is set in motion by a stepper motor (28BYJ-48 Stepper Motor) controlled by an Arduino Nano in order to position any filter exactly in front of the monochromatic camera lens as well as the RGB camera lens. The filter wheel is connected to the engine via a shaft cardan, as shown in Fig. 4(b). The stepper motor is connected to the digital GPIO output of Arduino Nano through a drive module that converts signals into analog values. The Arduino communicates via the USB serial connection with the Jetson

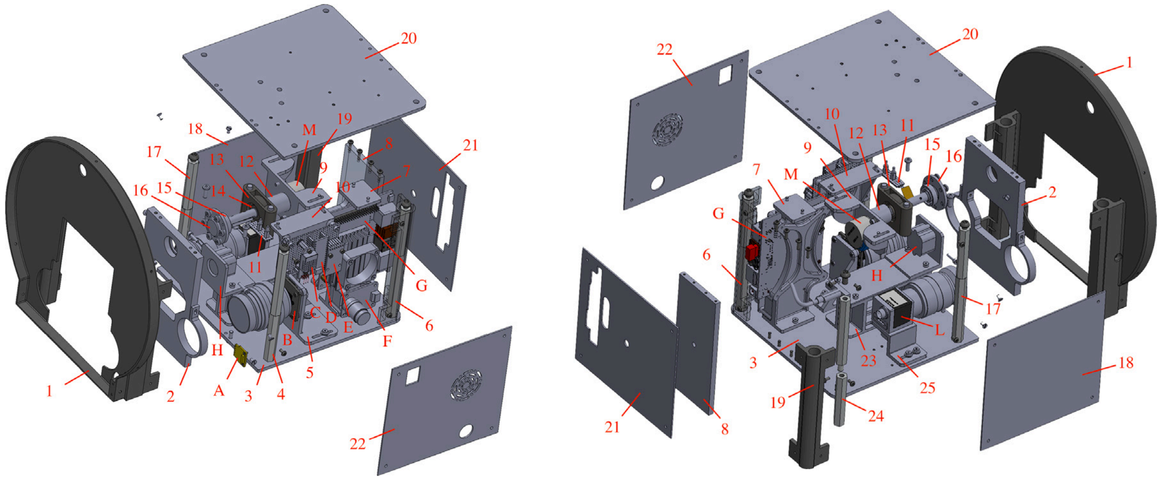

Fig. 5. CAD explosion view of the back part with all electronics and mechanical components. (A) Light sensor, (B) RGB camera, (C) Temperature and Relative Humidity, (D) Arduino Nano, (E) ULN2003 driver of stepper motor, (F) CO_2 sensor, (G) Jetson Nano, (H) Thermal camera, (M) Stepper Motor (28BYJ-48). Numbers indicate structural components: (1) Rear protective cap of the filter wheel, (2) Structural support for optics and drive shaft bearing, (3, 20) Bottom and top structural supports for sensors, (4,6,17,19) Lateral support poles, (5) Support for RGB camera, (7) Support for Jetson Nano, (8) Rear structural support with thread for tripod attachment screw, (9) Support for motor, (10) Support for sensors, (11) Support for wheel position detection sensor, (12) Coupling between motor and drive shaft, (13) Support for bearing, (14,15) Transmission shaft bearings, (16) Transmission shaft, (18,21,22) Lateral protection and closing plates of the MSX camera. (L) Monochromatic camera (Basler), (23) Support for thermal camera, (24) Component of the distancing pole, (25) Support for monochromatic camera.

Nano, the central control unit. This unit synchronizes processes such as wheel positioning and image acquisition for each filter. Before the image capture, the primary process tells the Arduino controller to move the filter wheel in the required position and waits for confirmation. Once the wheel is correctly positioned, the main process activates the image capture command. Since the system is designed to use two filters from two different cameras simultaneously (mono, RGB), they can be acquired at the same time but with different bands, depending on which filter each camera has in front.

To identify the initial position of the wheel, we have provided a perforated disk positioned on the Cardan that rotates together with the wheel and passes through a photodiode sensor. This facilitates the positioning of the filters. However, other approaches can be used to control the position of the filters, such as Hall effect sensor, lever switch, or contact circuit closer.

2.1.4. Mechanical structure: electronic central unit of MSX

Figs. 4(a), 4(b) and 5 show the CADs design from different perspectives to better distinguish the various components. As can be seen, the entire structure is designed in two units that interlock with each other to make the most of the space. The first unit contains the rotating wheel with the filters; the second unit has all the imaging sensors (monochromatic, RGB, and thermal), environmental sensors, processing units (Arduino Nano), and the motor with the parts necessary to operate the mechanism.

The MSX camera also contains the Jetson Nano single-board computer as the central processing unit that control all process. It is enclosed on the sides by aluminum and steel plates, where the steel plates have a series of holes of various diameters that are useful both for fixing the various components inside the MSX camera and for attaching them to the tripod (photographic standard) in different positions.

The final dimensions of MSX camera are 26 cm × 26 cm × 20 cm (W × H × D) and a weight of 3.4 kg, as shown Fig. 6. This makes it easily transportable, with the possibility of mounting it on a tripod, drone, or rover to take measurements in open fields or greenhouses.

3. Design files summary

Design filename	File type	Open source license	Location of the file
Multispectral camera (MSX)	CAD (.easm)	CERN-OHL-S	zenodo.org
Circuit diagram	.png	CERN-OHL-S	zenodo.org
MSX Software	Linux app	BSD-2-Clause “Simplified”	zenodo.org
Motor and sensors control	Arduino Software (.ino)	BSD-2-Clause “Simplified”	zenodo.org
User Guide	(.pdf)	BSD-2-Clause “Simplified”	zenodo.org

- The *Multispectral camera MSX* is a 3D CAD file of the multispectral camera with filters wheel, as shown Fig. 6.
- The *Circuit diagram* is the schematics of connection between sensors and Arduino Nano, see Fig. 8.

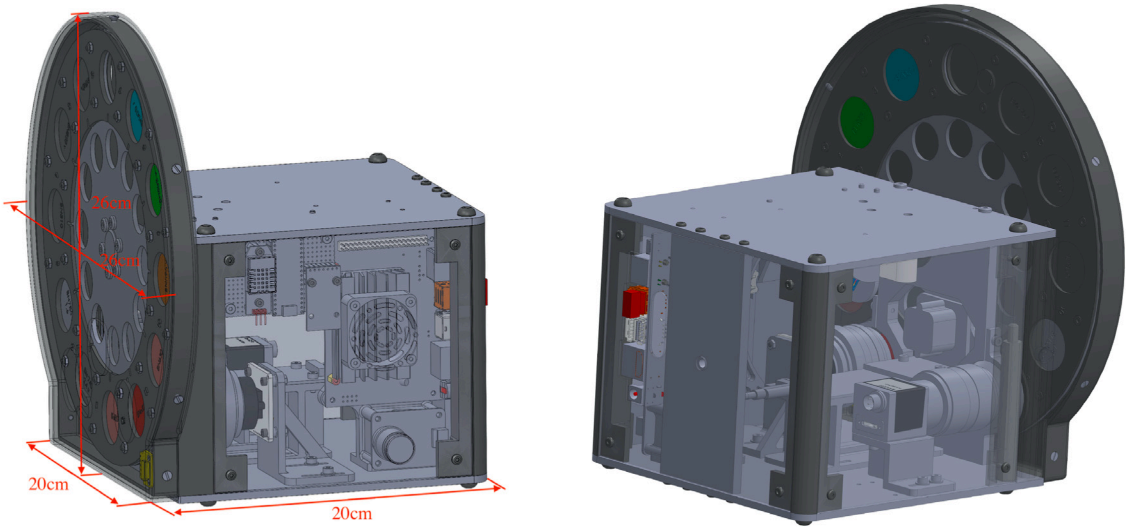

Fig. 6. CAD view of developed MSX multispectral camera with filter wheel.

- The *MSX Software* is the developed software for controlling all sensors of multispectral camera and image acquisition.
- The *Motor and sensors control* is a script for Arduino which controls the motor and the sensors (temperature, relative humidity, CO_2 and light intensity)
- *User Guide* is a comprehensive use manual for the MSX multispectral camera.

4. Bill of materials summary

ID	Component	Number	Cost unit/€	Source of materials	Material type
c1	Narrow band pass filters ⌀28 mm	11	167	MidOpt	Optics
c2	Basler aca2040-90umNIR	1	1290	Basler	Electronics
c3	Raspi HQ Cam	1	56	rs-online	Electronics
c4	Jetson Nano Kit	1	149	rs-online	Electronics
c5	Micro SD memory, 256 Gb	1	45	rs-online	Electronics
c6	Arduino Nano	1	22	rs-online	Electronics
c7	Stepper Motor 28BYJ-48	1	5	techmaker	Electronics
c8	Cables	15	10	rs-online	Electronics
c9	Sensor T/RH (DHT22)	1	11	rs-online	Electronics
c10	Sensor Light (BH1750)	1	11	rs-online	Electronics
c11	Sensor CO_2 (SEN0159)	1	50	rs-online	Electronics
c12	Inox Steel components 18 cm or 18 mm	1	20		Metal
c13	Support for Filters	2	10		3D Printing
c14	Protection for Wheel	2	10		3D Printing
c15	Sensors supports	5	15		3D Printing
c16	M5 screws	x	10	rs-online	Metal
c16	M3 screws	x	10	rs-online	Metal
c17	keyboard/mouse	1	30	rs-online	Electronics
c18	Monitor	1	150	rs-online	Electronics
c19	Power Station*	1	449	bluettipower	Electronics

5. Build instructions

To assemble the MSX camera, it is necessary to follow a specific order, starting from the back part (cubic shape) and ending with the wheel with filters.

The camera is equipped with a monitor for the visualization of the ROI that the camera acquires, connected by HDMI cable to MSX, a keyboard with a trackpad for input interaction, and a 5 V 4 A power supply cable.

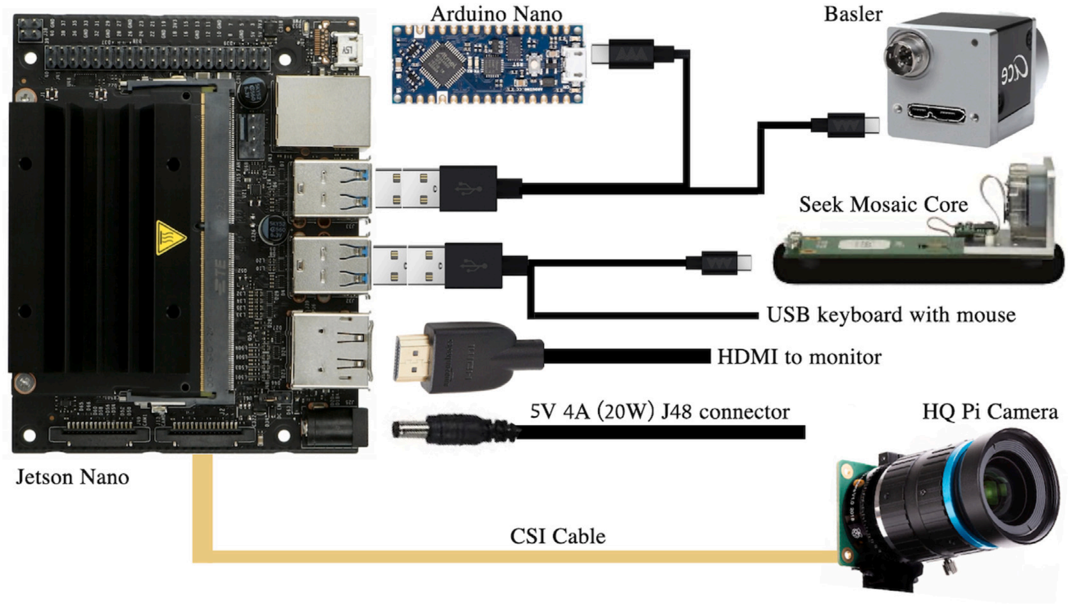

Fig. 7. Connection between Jetson Nano, sensors, monitor, USB keyboard with mouse and 5 V 4 A (20 W) power supply barrel connector J48.

5.1. Hardware assembly

Before starting the assembly of the structural part of the MSX camera, we recommend preparing the filter wheel with the filters and the various sensors connected to their supports. To assemble the filter wheel (Fig. 4(a)) the screws are inserted into the holes of components (5) and (4), then they are placed on a horizontal plane with component (5) facing downwards.

Each filter slot, is marked with a number ranging from 1 to 12 on the outer sides of the components (2) and (5), and to facilitate their correct positioning, we have added a small hole through the components (2), (4), and (5). Next, the filters are placed in their slots. We have set the BN470 filter in the first position and the BN532 in the second position, and so incrementally for the subsequent filters, except for position 12, where no filter is inserted, to allow all wavelengths to pass through and to do RGB imaging.

The sensors are connected to their respective supports, such as component (5) and (B) RGB camera with its optics, see Fig. 5; component (7) with (F) CO_2 sensor and with (G) Jetson Nano; component (9) and (M) stepper motor; component (25) and (L) Monochromatic camera. The component (10) is equipped with a drill plate to facilitate the layout of the electrical circuits connecting all the sensors and motor to the Arduino. The circuit diagram is shown in Fig. 8. Finally, the temperature and relative humidity sensors (C), Arduino Nano (D), and LN2003 driver of the stepper motor(F) are connected.

To assemble the MSX camera, it is recommended to start at the rear and join the components with the numbers (1), (2), (3), (4), and (17) together using screws, see Fig. 5.

The component (23) is connected to component (3) and the thermal camera (H), continue with components (5 + B), (7 + G), (F), (25 + L), (6) and (19) to the lower plate, component (3); and components (9 + M), (10 + C), (D), and (E), (11) and (13 + 14) to the upper plate, component (20).

The next steps, consist of fastening component (20) using screws to components (4), (6), (17), (19), after connect component (15) bearing with (16) transmission shaft and passing it through the bore and bearing housing located in component (2). Then it is necessary to connect the drive shaft to the motor via a coupling component (12) and attach components (8) to components (3), (20) and components (18), (21), (22) to components (1), (6), (19).

Finally, the previously assembled filter wheel is attached to component (16 — the drive shaft) using screws, where a through-hole is located nearby to align the wheel in the same fixing position with the initial position reference fixed on the cardan shaft for the position sensor. Then, component (1) is fastened to component (7) using screws; see Fig. 4(a).

5.2. Electronic components connections

The Jetson Nano is connected to the imaging sensors and the Arduino Nano via USB and CSI cable as shown in Fig. 7. The Arduino Nano is connected to the stepper motor, which moves the filter wheel.

Fig. 8 shows the circuit connecting the Arduino Nano, the stepper motor, and the environmental sensors (temperature, relative humidity, carbon dioxide, and light intensity).

Table 4 lists the GPIO PIN names between the wire connections. The Arduino Nano is connected to the Jetson USB 3.1 port through a UBS cable.

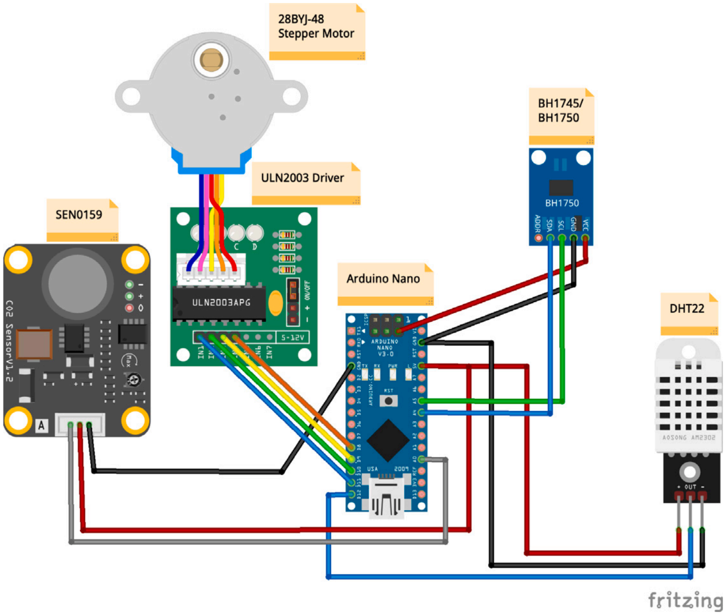

Fig. 8. Circuit connection between Arduino Nano, sensors, and stepper motor.

Table 4
Pinouts connection between Arduino Nano, sensors, and stepper motor.

GPIO Arduino Nano	DHT22	SEN0159	BH1750	ULN2003
5V	+	+	+	
D12	OUT			
GND	GND/-	GND/-	GND	
A0		PIN 0		
A4			SDA	
A5			SCL	
D8				IN4
D9				IN3
D10				IN2
D11				IN1

5.3. Configuration and packages

The operating system for the Jetson Nano that needs to be installed can be found on the official website [25]. A micro-SD memory of at least 68 GB is required to install the Nvidia-recommended operating system installer. The next step is to mount the micro-SD in the dedicated slot on the Jetson Nano board, switch it on, and follow all the steps to install the operating system (Ubuntu Linux). Next, it is necessary to update and install the drivers for the cameras and Arduino. To do these steps, we have created a guideline with detailed files, which can be found in the repository under the name README, for the following components: Basler camera, CSI MIPI Raspberry QH camera, Seek Thermal camera, Arduino and the packages for the various sensors. After all the steps have been completed and checked, and there are no errors, the MSX software that manages the entire MSX multispectral system can be started up. Download the `MSXSoftware` (EXE file) from the repository, and before launching it, verify that the user has permission to execute; if not, run in terminal `chmod u+x MSXSoftware`. After the configuration and permission have been set, it is possible to run the program in the following way `./MSXSoftware` from the terminal or double-click on the icon. The instruction about how to use the MSX Software is described in a PDF file named User Guide.

6. Operation instructions

Start the camera and position it in front of the target. Run the MSX application and select the type of sensor to be used. Adjust the distance between the camera and the region of interest by adjusting the focal length of the optics until the optimum field focus is obtained and then perform the acquisition. Before taking thermal measurements, it is recommended to wait a few minutes after running the program MSX with the thermal sensor (LWIR) selected in the MSX user interface to reach the working temperature of the sensor. This step is essential to obtain precise temperature measurements.

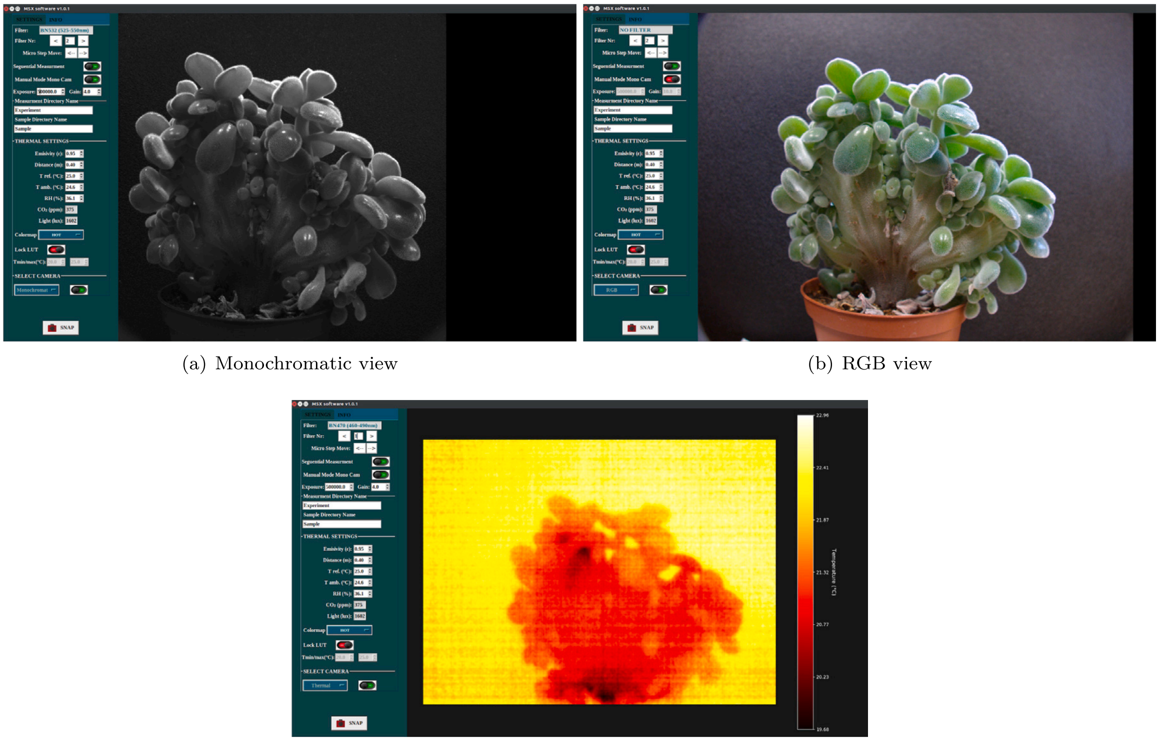

(a) Monochromatic view

(b) RGB view

(c) Thermal view

Fig. 9. User interface of MSX camera.

6.1. MSX Software

The MSX Software is implemented in Python using tkinter packages for the Graphical User Interface (GUI) and exported as a single application. This software let the user control all the imaging sensors and filter positions individually. The labels and buttons are on the left side of MSX GUI as shown in Fig. 9. Precise conversion from RAW values to Temperature values requires setting the necessary parameters in thermographic measurements [26], such as emissivity, distance, etc. The thermal maps are visualized in real-time, with the possibility of selecting the range of temperatures and optimizing the colormap to the dynamics of the target object. This Mosaic Core sensor is equipped with an internal diaphragm for automatic operation. It is a flat-fielding operation based on shuttering to compensate for temperature variation, pixel-to-pixel non-uniformity, and lens effects. In the central-right area, there is a view of live acquisition that the imaging sensor captures at each sample frame. The GUI is shown in Fig. 9, and the software's main functions are listed below.

`SNAP` It grabs the single frame and saves it in `.tiff` and, only for thermal image, also in `.png` format.

`< >` These buttons switch to the next and previous filter and update the filter label name with the wavelength bandpass description.

`<- ->` These buttons help to perform micro-movements of the filter wheel in case it is not ideally positioned in front of the optics.

`Sequential Measurement` If it is ON, after each acquisition, SNAP moves the filter wheel to the next filter; if it is OFF, it does not move, and multiple images can be acquired with the same filter.

`Manual Mode Mono Cam` If it is ON, the monochromatic camera exposure and gain values in Exposure/Gain labels can be setted; if it is OFF, the exposure and gain are in automatic mode.

`Thermal Settings` To set the experimental parameters for precise temperature measurements. These parameters are needed for the temperature conversion calculus of the raw data.

`Colormap` Allow to select the colormap for thermal visualization.

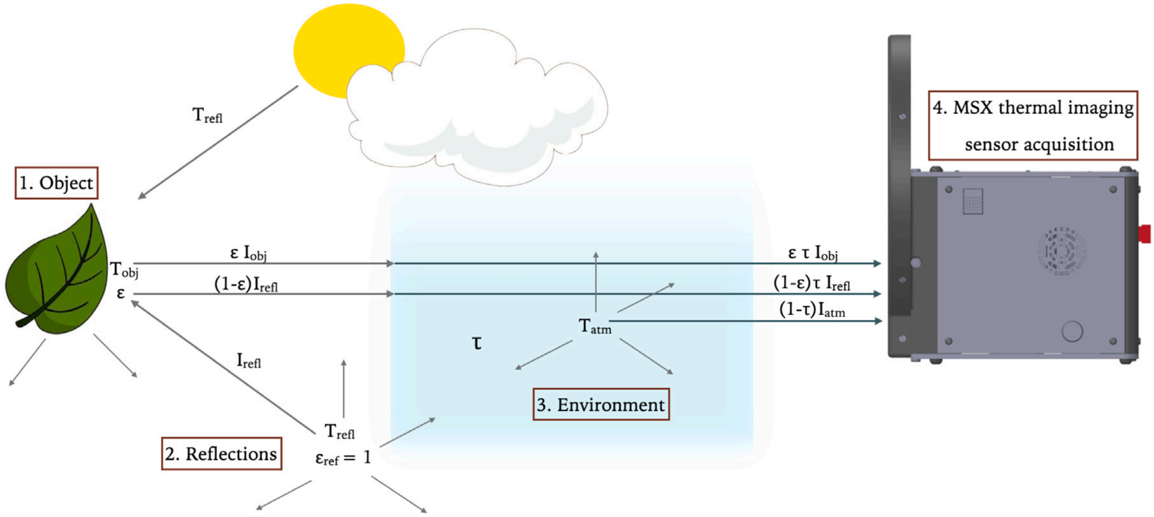

Fig. 10. Sketch of the components measured by the thermographic imaging sensor in a real environment: the total signal collected by the camera comes from object emission (1), object reflections (2), and atmosphere emission (3).

`Lock LUT` If it is ON, the temperature range to visualize the thermal sequence can be kept static in the Lookup Tables (LUT), i.e., the colormap; if it is OFF, the LUT is dynamic.

6.2. MSX camera measurements

During a measurement the multispectral camera MSX collects the radiation reflected in the VIS and NIR spectral bands with the CMOS RGB and Monochrome sensors and the total amount of LWIR radiation emitted with the Microbolometer. The reflected radiation components in the VIS–NIR range are separated into different bands by the narrowband filters, before reaching the imaging sensor.

Incident light is, in part, absorbed, reflected, or transmitted by matter. For example, in the case of plants, the component of reflected light in the VIS band that dominates in leaves is located around 500 nm, which corresponds to the color green, which is why we see green leaves. There are several methods to record and analyze these specific spectral signatures of matter, such as spectrometers and multi or hyperspectral imaging. In particular, through multispectral imaging, it is possible to acquire an area of interest in several smaller spectral bands using optical filters. The components of reflected radiation in the VIS and NIR band can be separated into different regions of the spectrum using narrowband filters, before the waves reach the imaging sensor (sensitivity 400–1000 nm) where they are acquired.

Also, all objects emit thermal radiation. The higher the temperature, the greater the energy carried by the photons and, respectively, the shorter their wavelength. Objects with temperatures between −40 °C and 150 °C have the highest peak emission in the wavelengths between 7.8 μm to 14 μm, i.e, LWIR thermal band. A sensitive LWIR-band sensor (microbolometer) is used to acquire the thermal radiation emitted by object at room temperature. This sensor also records the reflected and transmitted components from the surrounding environment, which must be taken into account for an accurate measurement, as schematized in Fig. 10, which includes the following contributions [27]:

1. emission from the object, related to its temperature T_{obj} and dependent on surface emissivity ε. It is computed as $\tau\varepsilon I(T_{\text{obj}})$, where τ is the medium transmissivity, and the function $I(T)$ comes from the calibration of the camera, i.e., the radiation collected from a blackbody radiator.
2. emission from environment sources reflected by the object. It is computed from the reflectivity $(1-\varepsilon)$ and an effective environment temperature, called the reflected temperature T_{ref}, therefore $\tau(1-\varepsilon)I(T_{\text{ref}})$.
3. emission from the atmosphere, computed as $(1-\tau)I(T_{\text{atm}})$.

The parameters ε, T_{ref}, T_{atm}, distance, and relative humidity must be input for the specific experiment (`Environment Settings`); the transmission coefficient τ is calculated by the software using the FLIR formula available in [28]. These parameters affect the calculation of the object temperature from raw thermal data. The accuracy of converting raw data to temperature values depends on the camera calibration provided by the manufacturer. The calibration of a thermal camera requires adequate equipment to perform measurements in controlled conditions of certified blackbody radiators.

Thermal emissivity of materials (ε): on the surface, an object has a specific thermal emissivity that varies with the type of material it is made of, the roughness of the surface, its temperature, and the wavelength of radiation. The emissivity coefficients of the most common materials are given in Table 5; more details on other materials can be found in the online Engineering ToolBox (2003) [29]. The emissivity values used for vegetation thermography are, on average, 0.957 ± 0.038 (mean ± SD) [30,31].

Table 5
Emissivity of some common materials ($T = 300\,\mathrm{K}$) in the LWIR range.

Materials	Emissivity (ε)
Black body	1
Plaster	0.98
Black Silicone Paint	0.93
Water	0.95–0.96
Asphalt	0.93
Concrete	0.85
Plant leaves	0.8–0.98
Wood	0.8–0.95
Aluminum Foil	0.04

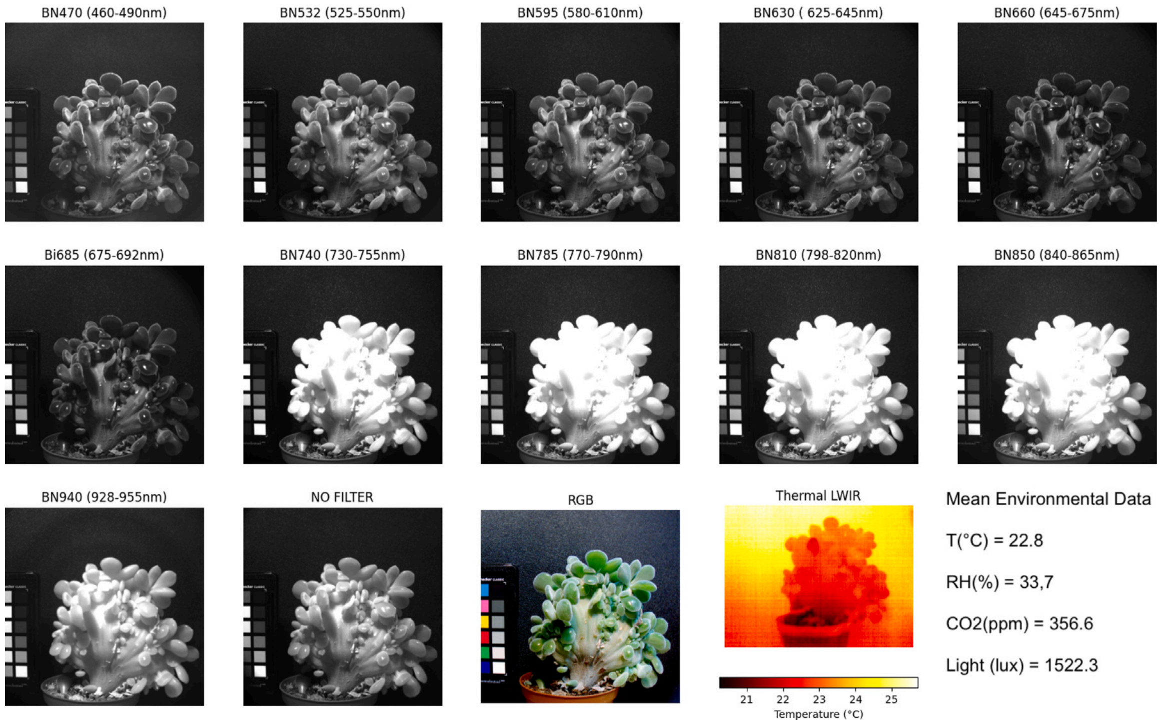

Fig. 11. Stack of images from MSX camera.

7. Validation

7.1. MSX camera data

The MSX output data is a stack of multispectral images in the VIS–NIR range, an RGB image, and a LWIR thermogram (Fig. 11). Each narrow band image is stored in tiff format (raw 12-bits) and named `FILTER_X`, with X the filter used for acquisition. The thermogram has a dual format for each acquisition, a tiff radiometric file, containing the temperatures, and a png file with the colormap and the colorbar applied for faster visualization. In addition, data from environmental sensors, such as temperature (°C), relative humidity (%), carbon dioxide (ppm) and light intensity (lux) are stored in the CSV format file, named `ENV_Data_DD_MM_YYY`. The software writes a new line to the CSV file for each acquisition, reporting the time and the environmental data.

All data are stored in a subfolder as a sample in the experiment folder, which you can set up in the GUI, ↦ `Sample Directory Name` and ↦ `Experiment Directory Name` respectively.

7.2. Spectra extraction from multispectral images

To evaluate the performance of the MSX camera, we performed a benchmarking with the VIS–NIR spectrometer using certified colorimetric targets with known spectra. We acquired a set of multispectral images for each standard and the spectrum with the spectrometer. Each image I was calibrated using a spectralon white reference with a certified reflectance R_{REF} of 99%. We selected a region of interest (ROI) on the reference color target and extracted the average reflectance value from each image in the multispectral stack. The reflectance value was estimated for each band using the following formula

$$\frac{I}{I_{\mathrm{REF}}} = \frac{R}{R_{\mathrm{REF}}} \tag{1}$$

where I_{REF} is the averaged image of the white reference. Fig. 12 shows the image data and an example of spectrum extracted from the multispectral stack. The result was then validated with the spectrometer. Fig. 13 shows the results obtained for all the colorimetric targets. The spectra estimated with the MSX camera are close to the spectra acquired with the spectrometer. Slight differences are observed as the MSX reflectance value is calculated through a wider spectral window (filter bandwidth around 40 nm) than the spectrometer resolution (2 nm). This demonstrates the accuracy of the MSX camera in faithfully extracting spectral information.

7.3. Applications in laboratory

Laboratory testing has highlighted the potential of the MSX multispectral camera to create a repeatable measurement protocol. These preliminary tests are critical for exploratory studies to identify the most relevant biological markers and optimal spectral bands, especially for plant diseases. In a laboratory setting it will be possible to arrange samples with specific diseases under the best conditions to identify the most relevant spectral bands. It is essential to be able to carry out a comprehensive laboratory analysis of spectral signatures before moving into open field conditions, such as a greenhouse or open field, since several factors can negatively affect the measurements.

Fig. 14 shows, as example, the exploration of the spectral signature in a plant using the multispectral stack; the typical reflectance of the chlorophyll in the NIR region is clearly observed. The procedure of extracting coarse spectra from multispectral imaging is well-recognized in the NDT field, especially when working on nonhomogeneous samples [7], and turns out to be very promising in plant imaging.

A few measurements with the MSX camera on plants with some leaf areas affected by pathology are shown in Fig. 15. In the bands of the VIS region, especially with the BN685 filter (675–692 nm), the areas where the infection has reached the leaves are clearly detected (higher reflectance); the healthy leaf areas show lower intensity as the chlorophyll absorbs light in these wavelength band. The BN810 filter (798–820 nm) shows well the necrotic area (lower reflectance) where there is no more chlorophyll, while the healthy leaves are characterized by the high reflectance of the chlorophyll in the NIR.

Fig. 15(c) shows the Normalized Differential Vegetation Index (NDVI), estimated from the NIR and red (R) channel as follows

$$\mathrm{NDVI} = \frac{\lambda_{\mathrm{NIR}} - \lambda_{\mathrm{R}}}{\lambda_{\mathrm{NIR}} + \lambda_{\mathrm{R}}} \tag{2}$$

where λ_{NIR} is the reflectance in the NIR wavelengths (790 nm $\pm$ 20 nm) and λ_{R} is the reflectance in the red wavelengths (680 nm $\pm$ 20 nm). NDVI values generally range between -1 and $+1$, where a value of 1 indicates maximum vegetation cover with high vigor. It is possible to see areas of lower plant vigor, perhaps due to phytopathology or nutrient stress, as it is commonly used as a direct indicator of vegetation health and growth [32].

7.4. Applications in open field

We tested the MSX camera in the open field to collect multispectral data in a vineyard. From the image stack, it is possible to estimate various plant indices, cross-referenced with environmental data. Fig. 16 shows the setup in a vine field with the calibration target positioned in scene, together with some collected data in the reflectance NIR band and emissive LWIR band, using the sun light as source. Fig. 17 shows, as application, one of the results that can be obtained from spectral imaging, i.e., the calculation of the Normalized Difference Red Edge (NDRE). The NDRE index is similar to NDVI but uses the NIR (790 nm $\pm$ 20 nm) ratio and the red edge (720 nm $\pm$ 20 nm) channels. Potentially it can be used for leaf chlorophyll content, plant vigor, stress detection, fertilizer demand, nitrogen uptake, diseased plants, pest-infested plants, nutritional deficiencies, and damaged plants [32].

This demonstrates the potential for application of the MSX device even in the open field, which can help the farmer to promptly identify the areas of the field that require intervention.

It is worth mentioning that, measurements in an open field are not easy as several factors can negatively affect the measurements, including non-uniform lighting or the sun's rays at the camera, which can saturate the signal acquired by the sensor. If it rains, the information collected may vary depending on the water deposited on the sample. Some samples can be covered by other samples (e.g., other leaves), depending on the direction of growth of the branches. However, this last aspect can be reduced by acquiring from different perspectives.

Table 6 summarizes the most relevant vegetation indices that can be computed with the multispectral camera dataset.

(a) Multispectral images

(b) RGB image

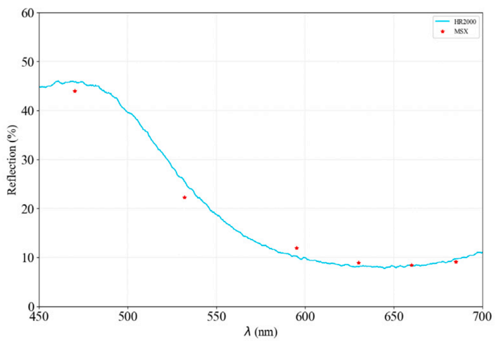

(c) Spectrum

Fig. 12. Cyan color target acquired in the multispectral bands (a), RGB image (b), comparison of the spectrum acquired with the spectrometer Ocean Optics HR2000 and the reflectance computed from the calibrated multispectral stack. (For interpretation of the references to color in this figure legend, the reader is referred to the web version of this article.)

7.5. Conclusion

We have implemented an innovative multispectral imaging system (named MSX) for precision agriculture, which is based on three core camera systems in the optical and thermal ranges and is optimized for close imaging of plants. Two CMOS sensors (monochrome and RGB) are coupled to a rotating wheel with interchangeable filters for optimizing in-band spectral imaging in the VIS–NIR range, while a compact microbolometer allows LWIR thermography. A set of sensors acquire environmental data (T, RH, CO2, and Lux). We designed the camera following the configuration based on filter-wheel as this approach allowed the use of high-performance sensors and optics.

Compared with the multispectral cameras available for agriculture, which are mainly designed for drones, the advantages of proposed system are modularity, low-cost, and the high-quality acquisition in a close-up setup (from tens of meters down to 1 m) together with the inline monitoring of environmental parameters. The system is suitable to be mounted on rovers in order to acquire spatial distribution of CO_2 concentration values, light intensity, temperature, and relative humidity to reconstruct a map. The idea

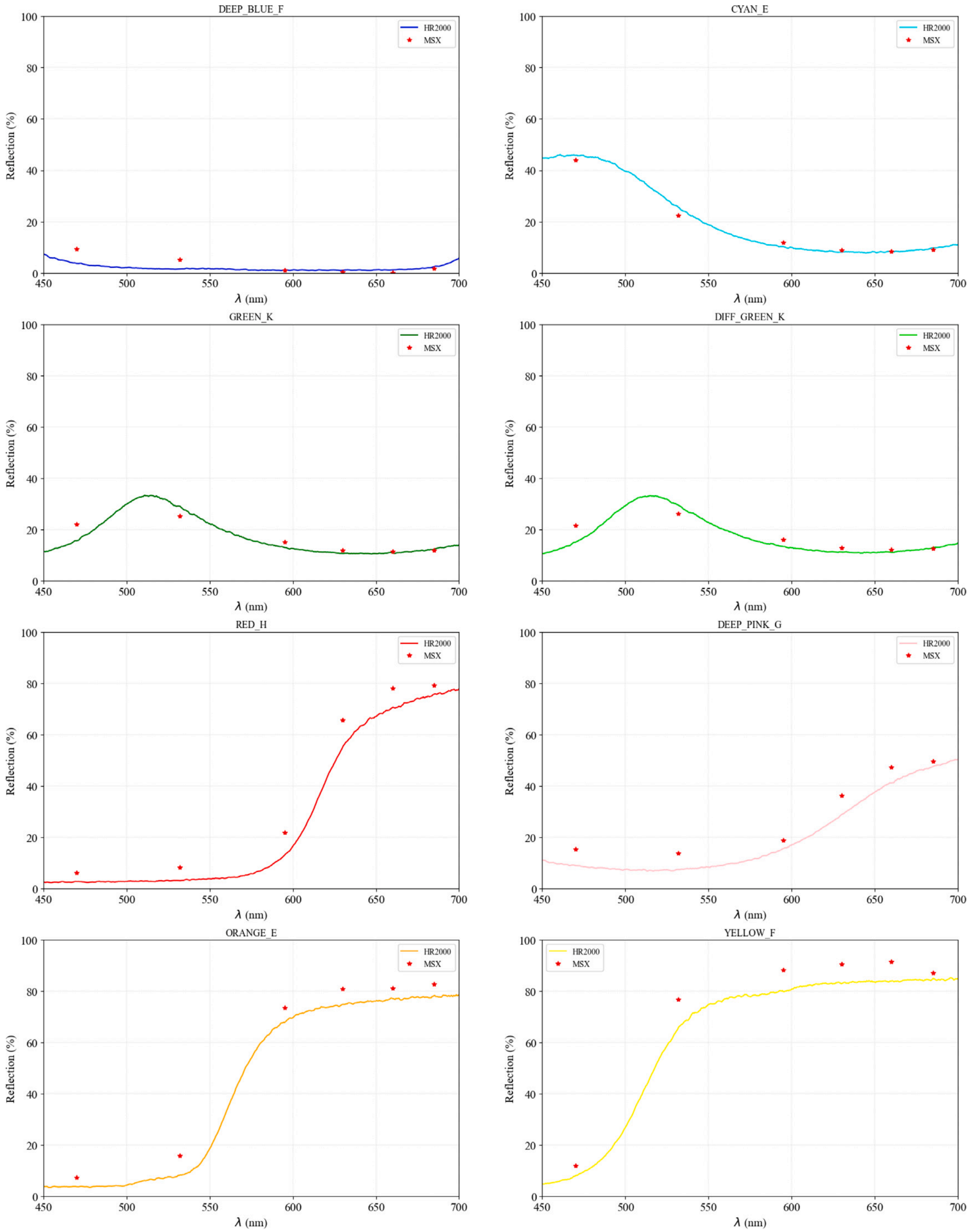

Fig. 13. Reference color target spectra acquired with the spectrometer Ocean Optics HR2000 and computed from the calibrated multispectral images acquired with the MSX camera.

is that plants are dynamic systems that respond to the environment, and our camera can provide a more comprehensive monitoring through integrated data processing.

The system is easily transportable and can be used on a tripod, on agricultural machinery, on UGVs in greenhouses and open fields to make measurements even on individual plants with high spatial resolution.

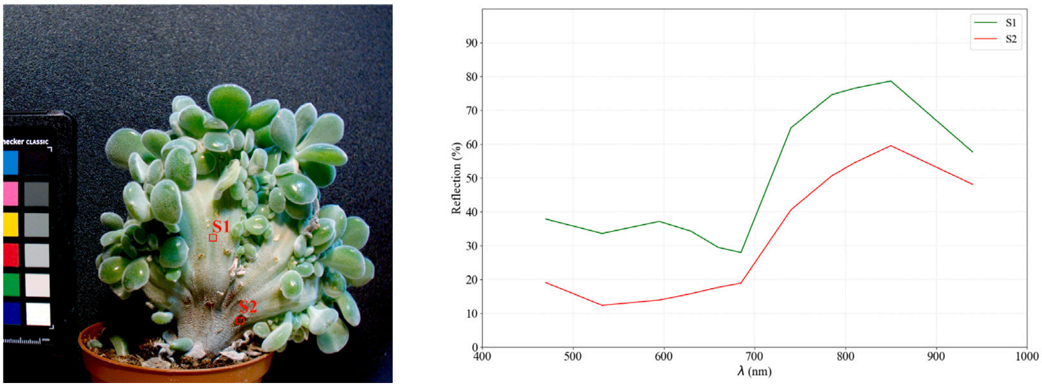

(a) RGB image (b) Spectrum

Fig. 14. Spectra extracted from a multispectral image stack (MSX camera) in a plant. Chlorophyll absorbs the blue (420–450 nm) and red (620–680 nm) wavelengths but reflects in the NIR region.

(a) Filter BN685 (b) Filter BN810 (c) NDVI

Fig. 15. Images acquired in laboratory with the MSX multispectral camera. (a) BN685 filter (675–692 nm) shows higher reflectance where the infection has reached the leaves, (b) while the BN810 filter (798–820 nm) shows the necrotic areas (lower reflectance) where there is no more chlorophyll. (c) NDVI is the Normalized Difference Vegetation Index.

(a) MSX system (b) VIS image (c) NIR reflectogram (d) LWIR thermogram

Fig. 16. (a) Open field acquisition with the MSX multispectral camera. Images (detail on healthy vegetation): (b) VIS (RGB), (c) NIR (reflectance band, Filter BN850), (d) Thermogram (emissive LWIR band, with the following parameters ϵ=0.95, Distance = 0.5 m, T_{ref} = 30 °C, T_{amb} = 27.9 °C, RH = 35.6%).

(a) RGB image (b) NDRE

Fig. 17. Computation of Normalized Difference Red Edge (NDRE) to map the healthy vegetation.

Table 6
Summary of principal vegetation indices.

Index	Formula	Related to	Reference
Simple ratio	$\frac{R_{800}}{R_{670}}$	Biomass, leaf area	Birth and McVey (1968) [33]
Normalized Difference Vegetation Index (NDVI)	$\frac{R_{800}-R_{670}}{R_{800}+R_{670}}$	Biomass, leaf area	Rousse et al. (1974) [34]
Normalized Difference Red Edge Index (NDRE)	$\frac{R_{850}-R_{715}}{R_{850}+R_{715}}$	chlorophyll content and nitrogen inside the leaves.	Gitelson and Merzlyak (1998) [35]
Crop Water Stress Index (CWSI)	$\frac{T_{plant}-T_{wet}}{T_{dry}+T_{wet}}$	Water content	Jackson, 1981 [36]
Structure insensitive vegetation index (SIPI)	$\frac{R_{800}-R_{445}}{R_{800}+R_{680}}$	Ratio carotenoids/chlorophyll a	Penuelas et al. (1995) [37]
Pigments specific simple ratio (PSSRa)	$\frac{R_{800}}{R_{680}}$	Chlorophyll (a/b) content	Blackburn (1998) [38]
Anthocyanin reflectance index (ARI)	$\frac{1}{R_{550}}$	Anthocyanin	Gitelson et al. (2001) [39]

The MSX camera and measurement processes have been experimentally validated in the laboratory and open field. The spectral signature of the plant can be investigated from the multispectral image stack, from which a punctual spectrum in the VIS–NIR can be extracted in different regions. This spectral mapping, performed at high spatial resolution and at coarse spectral resolution, allows us to select the optimal bands for feature detection in the case of interest. Using multispectral imaging, various vegetation indices, such as NDVI, NDRE, VI, etc., can be calculated to evaluate the health status of plants. At the same time, thermal data can identify uneven watering areas and the early stage of disease development in plants.

Future work will concern the exploitation of the multispectral VIS–NIR dataset for the precision agriculture applications through image mapping. Typical vegetation indices have been originally developed for satellite imagery and further investigation is necessary for close-up imaging of the single plants [12]. Further work will regard the integration of MSX imaging with AI to process the huge amount of collected data on field.

CRediT authorship contribution statement

Dumitru Scutelnic: Writing – original draft, Software, Investigation, Data curation. **Riccardo Muradore:** Writing – review & editing, Supervision, Methodology, Conceptualization. **Claudia Daffara:** Writing – review & editing, Writing – original draft, Supervision, Methodology, Conceptualization.

Ethics statements

This work did not involve the use of human or animal subjects.

Declaration of competing interest

The authors declare that they have no known competing financial interests or personal relationships that could have appeared to influence the work reported in this paper.

Acknowledgments

This research was carried out within the Decree of the Ministry of University and Research No. 1061 of August 10, 2021, to allocate FSE REACT-EU resources for the PON "Ricerca e Innovazione" 2014-2020. It was also carried out as part of the PNRR research activities of the consortium iNEST (Interconnected North-East Innovation Ecosystem) funded by the European Union Next-GenerationEU (Piano Nazionale di Ripresa e Resilienza (PNRR) Missione 4 Componente 2, Investimento 1.5 D.D. 1058 23/06/2022, ECS_00000043). This manuscript reflects only the Authors views and opinions, neither the European Union nor the European Commission can be considered responsible for them.

References

[1] FAO, Food, The Future of Food and Agriculture–Trends and Challenges, Annual Report 296, 2017, pp. 1–180, https://www.fao.org/3/i6583e/i6583e.pdf.
[2] N. Telagam, N. Kandasamy, M. Arun Kumar, Review on smart farming and smart agriculture for society: Post-pandemic era, in: C. Chakraborty (Ed.), Green Technological Innovation for Sustainable Smart Societies, Springer, Cham, 2021, http://dx.doi.org/10.1007/978-3-030-73295-0_11.
[3] C. Daffara, R. Muradore, N. Piccinelli, N. Gaburro, T. de Rubeis, D. Ambrosini, A cost-effective system for aerial 3D thermography of buildings, J. Imag. 6 (2020) 76, http://dx.doi.org/10.3390/jimaging6080076.
[4] M.-A. Ilişanu, F. Moldoveanu, A. Moldoveanu, Multispectral imaging for skin diseases assessment—State of the art and perspectives, Sensors 23 (2023) 3888, http://dx.doi.org/10.3390/s23083888.
[5] Feiyan Ma, Mingzhen Yuan, Igor Kozak, Multispectral imaging: Review of current applications, Surv. Ophthalmol. (ISSN: 0039-6257) 68 (5) (2023) 889–904, http://dx.doi.org/10.1016/j.survophthal.2023.06.004.
[6] C. Daffara, S. Parisotto, P.I. Mariotti, Mid-infrared thermal imaging for an effective mapping of surface materials and sub-surface detachments in mural paintings: integration of thermography and thermal quasi-reflectography, in: Proc. SPIE 9527, 2015, http://dx.doi.org/10.1117/12.2184836.
[7] N. de Manincor, G. Marchioro, E. Fiorin, M. Raffaelli, O. Salvadori, C. Daffara, Integration of multispectral visible-infrared imaging and pointwise X-ray fluorescence data for the analysis of a large canvas painting by Carpaccio, Microchem. J. 153 (2020) http://dx.doi.org/10.1016/j.microc.2019.104469.
[8] D.C. Tsouros, S. Bibi, P.G. Sarigiannidis, A review on UAV-based applications for precision agriculture, Information 10 (2019) 349, http://dx.doi.org/10.3390/info10110349.
[9] A. Bannari, D. Morin, F. Bonn, A.R. Huete, A review of vegetation indices, Remote Sens. Rev. 13 (1) (1996) 95–120, https://d10.1080/02757259509532298.
[10] N.S. Beisel, J.B. Callaham, N.J. Sng, D.J. Taylor, A.L. Paul, R.J. Ferl, Utilization of single-image normalized difference vegetation index (SI-NDVI) for early plant stress detection, Appl. Plant Sci. 6 (10) (2018) http://dx.doi.org/10.1002/aps3.1186.
[11] Y. Osroosh, L.R. Khot, R.T. Peters, Economical thermal-RGB imaging system for monitoring agricultural crops, Comput. Electron. Agric. 147 (2018) 34–43, http://dx.doi.org/10.1016/j.compag.2018.02.018.
[12] D. Radočaj, A. Šiljeg, R. Marinović, M. Jurišić, State of major vegetation indices in precision agriculture studies indexed in web of science: A review, Agriculture 13 (2023) 707, http://dx.doi.org/10.3390/agriculture13030707.
[13] Y. Zeng, D. Hao, A. Huete, et al., Optical vegetation indices for monitoring terrestrial ecosystems globally, Nat. Rev. Earth Environ. 3 (2022) 477–493, http://dx.doi.org/10.1038/s43017-022-00298-5.
[14] S.D. Khirade, A.B. Patil, Plant disease detection using image processing, in: 2015 International Conference on Computing Communication Control and Automation, Pune, India, 2015, pp. 768–771, http://dx.doi.org/10.1109/ICCUBEA.2015.153.
[15] X. Rui, C. Li, S. Bernardes, Development and testing of a UAV-based multi-sensor system for plant phenotyping and precision agriculture, Remote Sens. 13 (17) (2021) 3517, http://dx.doi.org/10.3390/rs13173517.
[16] A. Morales, R. Guerra, P. Horstrand, M. Diaz, A. Jimenez, J. Melian, S. Lopez, J.F. Lopez, A multispectral camera development: From the prototype assembly until its use in a UAV system, Sensors 20 (2020) 6129, http://dx.doi.org/10.3390/s20216129.
[17] M. Rosenberger, R. Celestre, Smart multispectral imager for industrial applications, in: 2016 IEEE International Conference on Imaging Systems and Techniques, IST, Chania, Greece, 2016, pp. 7–12, http://dx.doi.org/10.1109/IST.2016.7738189.
[18] Joan Vila, Javier Calpe, Filiberto Pla, Luis Gómez, Joseph Connell, John Marchant, Javier Calleja, Michael Mulqueen, Jordi Muñoz, Arnoud Klaren, SmartSpectra: Applying multispectral imaging to industrial environments, Real-Time Imaging (ISSN: 1077-2014) 11 (2) (2005) 85–98, http://dx.doi.org/10.1016/j.rti.2005.04.007.
[19] Dafne Cimino, Giacomo Marchioro, Paolo De Paolis, Claudia Daffara, Evaluating the integration of Thermal Quasi-Reflectography in manuscript imaging diagnostic protocols to improve non-invasive materials investigation, J. Cult. Herit. (ISSN: 1296-2074) 62 (2023) 72–77, http://dx.doi.org/10.1016/j.culher.2023.04.009.
[20] Lei Deng, Zhihui Mao, Xiaojuan Li, Zhuowei Hu, Fuzhou Duan, Yanan Yan, UAV-based multispectral remote sensing for precision agriculture: A comparison between different cameras, ISPRS J. Photogramm. Remote Sens. (ISSN: 0924-2716) 146 (2018) 124–136, http://dx.doi.org/10.1016/j.isprsjprs.2018.09.008.
[21] George Themelis, Jung Sun Yoo, Vasilis Ntziachristos, Multispectral imaging using multiple-bandpass filters, Opt. Lett. 33 (2013) 1023–1025, http://dx.doi.org/10.1364/OL.33.001023.
[22] M. Barjaktarovic, M. Santoni, L. Bruzzone, Design and verification of a low-cost multispectral camera for precision agriculture application, IEEE J. Sel. Top. Appl. Earth Obs. Remote Sens. 17 (2024) 6945–6957, http://dx.doi.org/10.1109/JSTARS.2024.3377104.
[23] K.L. Ebi, I. Loladze, Elevated atmospheric CO2 concentrations and climate change will affect our food's quality and quantity, Lancet Planet. Health 3 (2019) e283–e284, http://dx.doi.org/10.1016/S2542-5196(19)30108-1.
[24] M. Thompson, D. Gamage, N. Hirotsu, A. Martin, S. Seneweera, Effects of elevated carbon dioxide on photosynthesis and carbon partitioning: A perspective on root sugar sensing and hormonal crosstalk, Front. Physiol. 8 (2017) http://dx.doi.org/10.3389/fphys.2017.00578.
[25] Jetson Nano Developer Kit, https://developer.nvidia.com/embedded/learn/get-started-jetson-nano-devkit.
[26] D. Scutelnic, G. Marchioro, S. Siracusano, P. Fiorini, R. Muradore, C. Daffara, Thermal endoscope based on cost-effective LWIR camera cores, HardwareX 11 (2022) e00300, http://dx.doi.org/10.1016/j.ohx.2022.e00300.
[27] M. Vollmer, K.P. Möllmann, Infrared Thermal Imaging: Fundamentals, Research and Applications, second ed., Wiley-VCH Verlag GmbH & Co. KGaA, Weinheim, Germany, 2018, http://dx.doi.org/10.1002/9783527693306.
[28] W. Minkina, D. Klecha, Atmospheric transmission coefficient modelling in the infrared for thermovision measurements, J. Sens. Sens. Syst. 5 (2016) 17–23, http://dx.doi.org/10.5194/jsss-5-17-2016.

[29] Engineering ToolBox, Emissivity coefficients materials, 2003, https://www.engineeringtoolbox.com/emissivity-coefficients-d_447.html.
[30] C. Chen, Determining the leaf emissivity of three crops by infrared thermometry, Sensors 15 (5) (2015) 11387–11401, https://www.ncbi.nlm.nih.gov/pmc/articles/PMC4481894/.
[31] M.J.M. Harrap, S.A. Rands, Floral infrared emissivity estimates using simple tools, Plant Methods 17 (2021) 23, http://dx.doi.org/10.1186/s13007-021-00721-w.
[32] E.M. Barnes, et al., Coincident detection of crop water stress, nitrogen status and canopy density using ground based multispectral data, in: Proceedings of the Fifth International Conference on Precision Agriculture, Vol. 1619, No. 6, Bloomington, MN, USA, 2000.
[33] G.S. Birth, G.R. McVey, Measuring the color of growing turf with a reflectance Spectrophotometer1, Agron. J. 60 (6) (1968) 640–643, https://onlinelibrary.wiley.com/doi/pdf/10.2134/agronj1968.
[34] S.C. Freden, E.P. Mercanti, M.A. Becker, Third Earth Resources Technology Satellite-1 Symposium: The Proceedings of a Symposium Held By Goddard Space Flight Center at Washington, D.C. on December (1973) 10–14, Prepared at Goddard Space Flight Center, Scientific and Technical Information Office, National Aeronautics and Space Administration.
[35] A. Gitelson, M.N. Merzlyak, Quantitative estimation of chlorophyll-a using reflectance spectra: Experiments with autumn chestnut and maple leaves, J. Photochem. Photobiol. B 22 (1994) 247–252.
[36] R.D. Jackson, S.B. Idso, R.J. Reginato, P.J. Pinter Jr., Canopy temperature as a crop water stress indicator, Water Resour. Res. 17 (4) (1981) 1133–1138, https://onlinelibrary.wiley.com/doi/pdf/10.1029/WR017i004p01133.
[37] J. Penuelas, B. Frederic, I. Filella, Photosyn1995, 2013.
[38] G.A. Blackburn, Spectral indices for estimating photosynthetic pigment concentrations: A test using senescent tree leaves, Int. J. Remote Sens. 19 (1998) 657–675, http://dx.doi.org/10.1080/014311698215919, Publisher: Taylor & Francis.
[39] A.A. Gitelson, M.N. Merzlyak, O.B. Chivkunova, Optical prop- erties and nondestructive estimation of anthocyanin content in plant leaves, Photochem. Photobiol. 74 (1) (2001) 38–45.

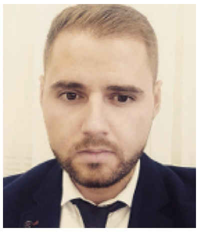

Dumitru Scutelnic has a Bachelor's degree in Bioinformatics and a Master's degree in Molecular and Medical Biotechnology at University of Verona.

After a research fellowship in optical and thermal technics for bio-medical application, he is now working at his Ph.D. project in Computer Science at the University of Verona.

Research interest are focused on the design and development of technologies and robotics in bio-medical and green applications for a better future.

Riccardo Muradore is Associate Professor at the Department of Engineering for Innovation Medicine of the University of Verona. He received the Laurea degree in Information Engineering in 1999 and the Ph.D. degree in Electronic and Information Engineering in 2003 both from the University of Padova (Italy). He held a post-doctoral fellowship at the Department of Chemical Engineering, University of Padova, from 2003 to 2005, working on statistical control and monitoring. Then he spent three years at the European Southern Observatory in Munich (Germany) as control engineer working on adaptive optics systems. In 2008 he joined the ALTAIR Robotics laboratory, University of Verona (Italy). He was the coordinator of the Horizon 2020 project SARAS (https://saras-project.eu/) and he is the local coordinator for UNIVR of the Horizon Europe GEYEDANCE project (https://geyedance.eu/) and the coordinator of the Horizon Europe ROBIOPSY project (https://robiopsy-project.eu/). His research interests include control and system theory, teleoperation, robotics, surgical robotics, predictive maintenance, networked control systems and adaptive optics.

Claudia Daffara is Associate Professor in Applied Physics at the University of Verona and Head of the Laboratory of Optical Devices and Advanced Techniques for Environment & Cultural Heritage (OpDATECH). She received a degree in theoretical physics from the University of Padova and a Ph.D. in applied physics from the University of Bologna, Italy. Before joining university in 2011, she held research positions at the CNR — National Institute of Optics (Florence, Italy) working in optics for heritage science.

Her research interests are applied physics and modeling in interdisciplinary fields. Research activities focus on developing optical techniques based on coherent and incoherent methods for nondestructive analysis of materials and surface metrology, including advanced imaging, infrared and thermal techniques, laser profilometry, and speckle methods. https://scholar.google.it/citations?user=SqaX6RYAAAAJ&hl=it